The Abdus Salam
International Centre for Theoretical Physics

EMAS 2008

8th EMAS Regional Workshop on

Electron Probe Microanalysis of Materials Today

Practical Aspects

including a session on

synchrotron-based microanalysis

19 - 22 April 2008

Adriatico Guesthouse
The Abdus Salam International Centre for Theoretical Physics
Trieste, Italy

Book of Abstracts

PERFORMANCE CHARACTERISTICS OF WDS AND EDS DETECTORS

Michael B. Matthews*

AWE Plc.
Aldermaston, Reading RG7 4PR, Great Britain
** matthm@hotmail.com*

INTRODUCTION

Traditionally the wavelength-dispersive spectrometer (WDS) has been the X-ray detector of the electron microprobe, and the energy-dispersive spectrometer (EDS) that of the scanning electron microscope (SEM). Now, of course, probably the majority of microprobes, and an increasing number of SEMs are fitted with both. The two detector types have very different performances and characteristics, and some understanding of these differences will help in making the most effective use of them. In this paper I hope to explain the main practical characteristics, and provide at least a starting point for a better understanding of how to best use the detectors. I have restricted the scope to only cover those characteristics which result from the detectors (e.g. not absorption or fluorescence in the sample), and only cover the most common types of detectors (e.g. no multi-layer synthetic diffraction 'crystals' and Silicon drift EDS detectors).

THE BASIC PRINCIPLES

Both systems are made up of a filter and a detector. The filter disperses the sample's emission X-ray spectrum which is then measured by the detector. As is suggested by their names the filter in WDS separates the X-rays according to their wavelength and in EDS by their energy. De Broglie's equation gives us a very simple relationship between an X-ray's energy and its wavelength:

De Broglie equation

$$E = hc/\lambda$$

where:
E is the energy of the X-ray,
λ is its wavelength,
h is Planck's Constant (6.626×10^{-34} Js),
c is the speed of light in a vacuum (3.0×10^{8} ms^{-1}).

Since h and c are both constants, the energy and wavelength are directly correlated:

$$E \propto 1/\lambda$$

i.e. as energy increases wavelength decreases. If energy doubles wavelength halves. For E in keV (1 keV = 1.6021 x 10^{-16} J) and λ in Å (1 Å = 1 x 10^{-9} m):

$$E = 12.396/\lambda$$

The result of this simple relationship is that the energy spectrum measured on the EDS can be converted into a wavelength spectrum by taking the inverse of the energy scale - the spectrum itself is essentially unchanged. The two detectors, then, are effectively measuring the same thing and the difference between them is more a result of their performances.

PART 1 - WAVELENGHT-DISPERSIVE SPECTROMETERS

The wavelength filter

The filter in a WDS is a regularly layered material, usually crystalline. This is commonly called a diffraction crystal, but can be more simply envisaged as a series of parallel reflecting surfaces. It uses the principle of constructive interference to selectively enhance some wavelengths and suppress all others. The Bragg equation gives us a relationship between wavelength, layer spacing, and angle of incidence (and reflection since the mechanism is symmetrical) at which constructive interference occurs:

Bragg equation

$$2d \sin\theta = n\lambda$$

where:
d is the layer spacing,
θ is the angle of incidence (and reflection),
n is an integer,
λ is the wavelength.

This is depicted in Fig. 1. If we envisage parallel waves of a given wavelength reflecting off the parallel layers at a given incidence angle. When the distance travelled by waves reflecting off the adjacent layers differs by exactly one wavelength the reflected waves line up. The resultant wave, produced by adding the reflected waves together, has the same wavelength but its amplitude is the sum off the amplitudes of the incident waves, so it's enhanced. The integer, n, is needed because the same constructive interference occurs if the distance is exactly

two or three, or any whole number, of wavelengths. Where the distance is not a whole number of wavelengths the reflected waves won't line up and the resultant summed waveform therefore won't be enhanced.

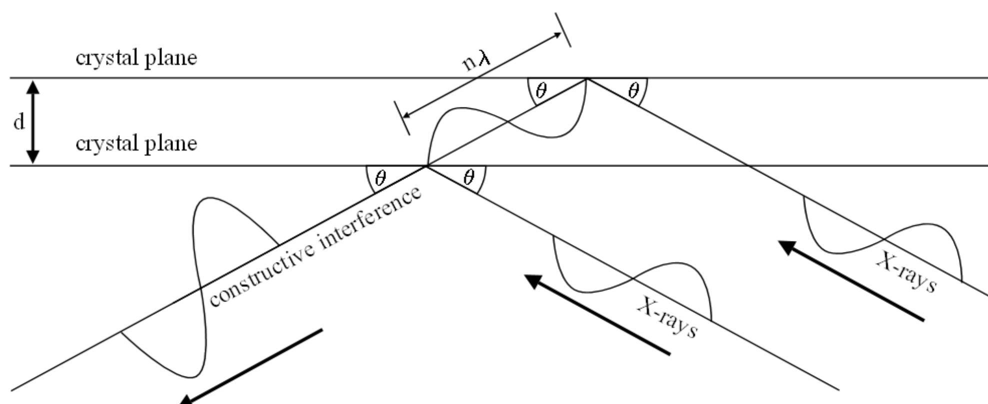

Fig. 1. Schematic showing condition of lattice spacing, incidence angle and wavelength for which the Bragg equation is satisfied and constructive interference of the emergent X-ray occurs.

If we change the angle of incidence we change the wavelength that satisfies the equation, and therefore the wavelength that is enhanced, and the spectrum of X-rays emitted from the sample can therefore be built up. The condition of constructive interference is very sensitive to d and θ. This produces the high resolving power of the WDS, but also causes some of its limitations.

The X-ray wavelengths of interest are generally of the order of 1 nm and we need d-spacings of the same order. Fortuitously this falls within the range of crystal lattices. Mechanical limitations mean that the incidence angle can only realistically be varied in the range $10^o \leq \theta \leq 70^o$, which is equivalent to $0.4d \leq \theta \leq 1.9d$. This is too small to cover the full range of wavelengths needed, so crystals with different d-spacing values are used to each cover a portion of the range (Fig. 2).

Geometry

To complete the WD spectrometer we need a detector to measure the intensity of X-rays coming from the diffraction crystal at each wavelength. This sits opposite the X-ray source (i.e. the sample) and at the same angle. If the X-rays reaching the crystal were parallel the geometry would be very simple, since the source and detector could be any distance from the crystal. However, since the source is essentially a point the optimum position for the detector is at the effective focus of the diffraction crystal and this will be when the source and detector are equidistant from the crystal (Fig. 3). This symmetrical geometry is defined by the circle

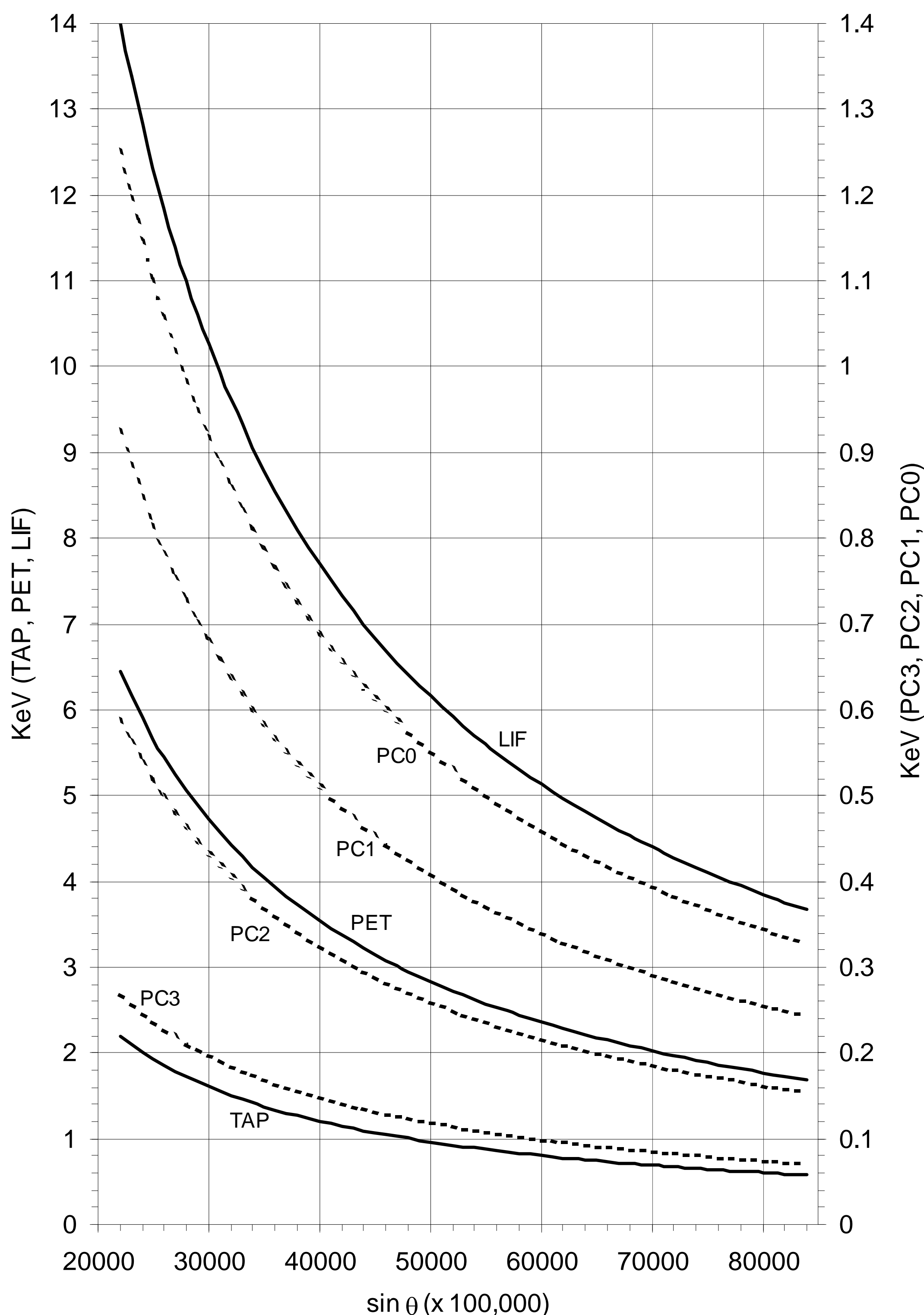

Fig. 2. Spectrometer position (expressed as the sine of the diffraction angle) versus energy curves for commonly used diffraction crystals.

that joins the source, crystal and detector together, called the Rowland circle of the spectrometer. Note, though, that there is nothing special about the fact that these three points can be joined by a circle. *Any* three points in space can always be joined by a circle. It is the

symmetry of the configuration that makes the Rowland circle useful and, as we shall see later, the size of this circle defines some of the properties of the spectrometer.

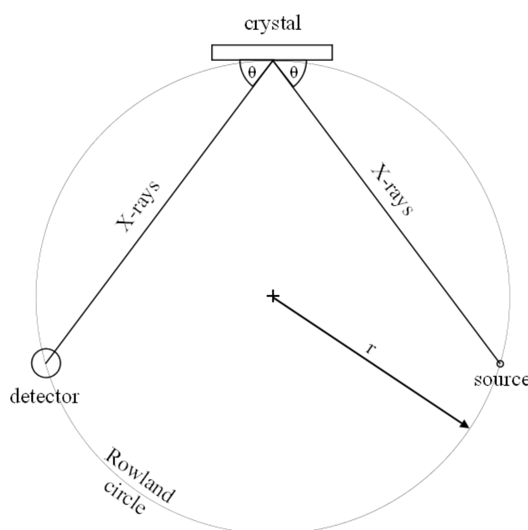

Fig. 3. Schematic showing the relationship between the Rowland circle and the source, diffraction crystal and detector of a WDS.

A more serious consequence of the X-ray source being a point is that the X-rays reaching the crystal are divergent. So for a flat crystal the diffraction angle will vary across the crystal and the Bragg equation will only be satisfied at one point, severely limiting its useable area. To maintain the same incidence angle over the face of the crystal, at least to a first approximation, the crystal planes need to be curved to a radius of $2r$, where r is the radius of the Rowland circle. This is known as Johann geometry. Unfortunately this does not fully correct for the effect since the face of such a crystal, although curved, diverges from the Rowland circle. A further improvement is made by grinding the face of the Johann crystal to a radius of r, creating what is termed a Johannson crystal. This more closely approaches the ideal in the plane of the Rowland circle, but doesn't correct for the loss of focus across the width of the crystal (Fig. 4). For this the crystal would need to be dished or doubly curved. Aside from the practical difficulties in producing such a crystal, the optimum radius of curvature in this second plane is a function of the angle of diffraction and so the curvature could only be optimised for a narrow range of angles. In fact the problems associated with grinding even the Johansson crystal without damaging the lattice mean that the Johann geometry is currently the most commonly used.

In both the Johann and Johannson geometries the incidence angle is *decreased* by deviation across the width of the crystal face, perpendicular to the Rowland circle. For Johann geometry the incidence angle also deviates in the line of the Rowland circle due to the unground crystal face deviating from the curve of the circle, but here the deviation produces an

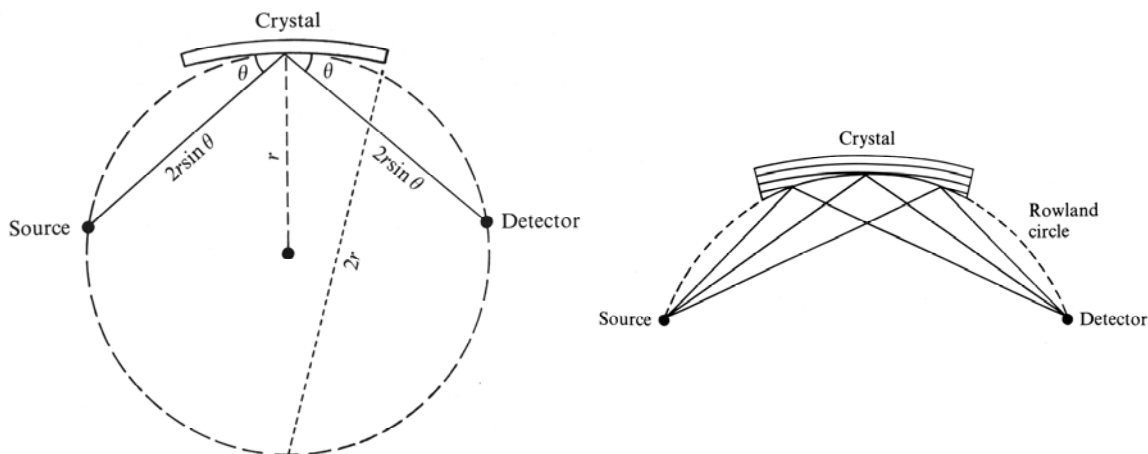

Fig. 4. Diagrams showing the geometries of Johann (left) and Johannson (right) crystals. For a Johann crystal the lattice planes are bent to a curve of $2r$, whilst in a Johannson crystal the curved crystal is ground to a radius r.

increase in the incidence angle. This means that, away from the centre point of a Johann crystal, the positive deviation produced along the length of the crystal will be exactly balanced at some point across the width of the crystal by the negative deviation resulting perpendicular to the Rowland circle. The distance of this point across the width of the crystal will increase with the distance along the circle. This will happen symmetrically, both either side of the Rowland circle and either side of the centre point in the line of the Rowland circle and produces an X-shape. This represents the focussed area of the crystal (Fig. 5). The ground curve of the Johannson crystal corrects for the deviation along the Rowland circle so the focussed area for this geometry is a band along the length of the crystal.

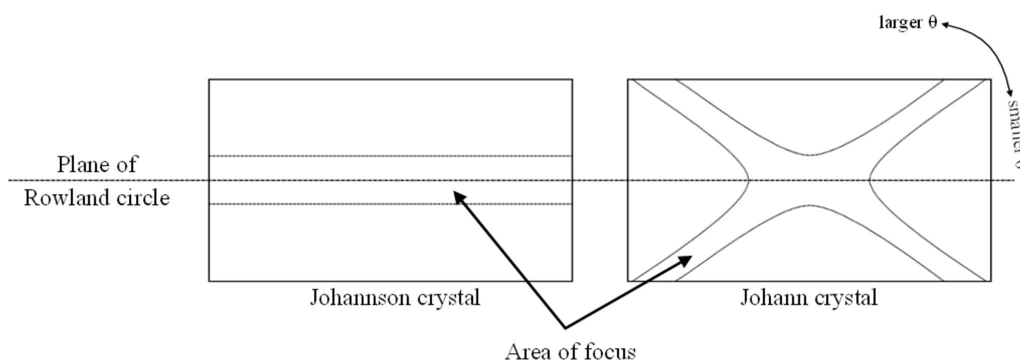

Fig. 5. Diagram showing the active or focussed zones on the face of Johann and Johannson crystals. On the Johann crystal the arms of the x-shaped pattern diverge or converge depending on the angle of incidence of the X-rays

Resolution

The band in which the crystal is said to be focussed (i.e. the angle of incidence satisfies the Bragg condition) is very narrow. Darwin (1914) calculated that for a perfect crystal it extends only a few seconds of arc either side of the plane of the Rowland circle. As shown below, the incidence angle decreases across the width of the crystal, given by the equation:

Deviation from the Bragg angle as a function of displacement across the crystal

$$\Delta\theta = \left(y/r\right)^2 / 4\sin 2\theta$$

where:
$\Delta\theta$ is the deviation from the Bragg angle,
y is the displacement perpendicular to the plane of the Rowland circle,
r is the radius of the Rowland circle,
θ is the angle of incidence.

For a given Bragg angle θ, this gives a maximum deviation, $\Delta\theta$, at the edge of the crystal where $y = a$ the half width of the crystal (Fig. 6).

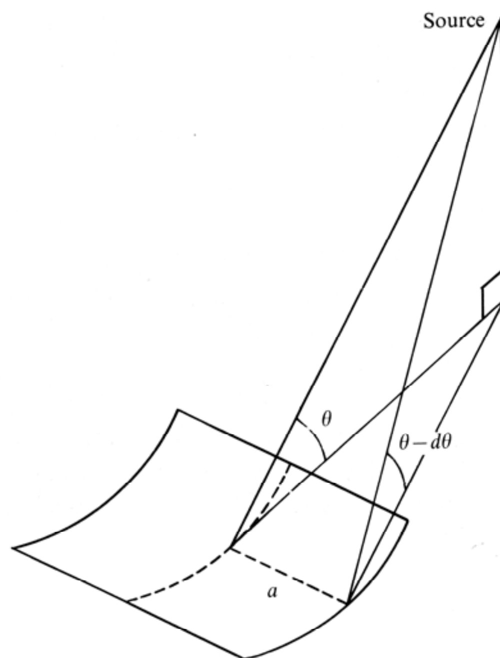

Fig. 6. Schematic showing the decrease in incidence angle on a crystal as a result of displacement across the width of the crystal.

The resolution of the crystal is determined by both the width of the band of focus and the value of $\Delta\theta$ at $y = a$. As a rule the $\Delta\theta$ term predominates so resolution is primarily governed by the value of a/r.

For a Johannson crystal the above equation is valid at any point along the length of the crystal. However, in Johann geometry an additional factor needs to be added due to the departure from the Rowland circle along its length:

Deviation from the Bragg angle as a function of displacement along a Johann crystal

$$\Delta\theta' = \frac{\left(x/r\right)^2}{4\tan\theta}$$

where:
$\Delta\theta'$ is the deviation from the Bragg angle,
x is the displacement along the plane of the Rowland circle,
r is the radius of the Rowland circle,
θ is the angle of incidence.

As above this is maximum for a given θ at the ends of the crystal, where $x = b$ its half length (Fig. 7). Fig. 8 shows the variation in the sum Bragg angle 'error' for both Johannson and Johann geometries over the range of incidence angles used in a WDS. From this we can see that the Johannson crystal has a shallow curve with a minimum at 45°. The 'error' for the Johann geometry, however, decreases strongly with increasing incidence angle, with its minimum value at the maximum incidence angle of the spectrometer. The practical result of this is that, for a Johann crystal, the resolution will always be better (smaller 'error') for peaks at a higher incidence angle. For example, a Si;Kα measured on a PET ($\theta = 54.53°$) will have a better resolution than when measured on a TAP ($\theta = 16.10°$).

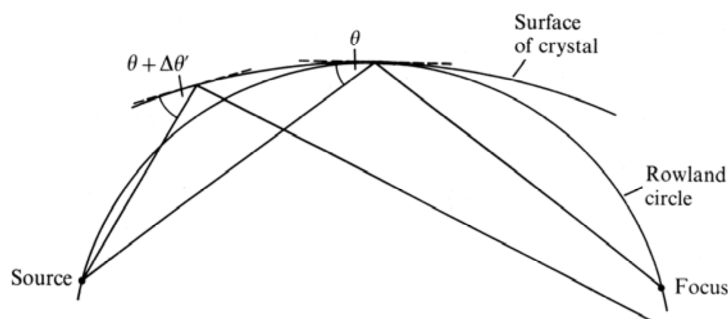

Fig. 7. Schematic showing the increase in incidence angle on a crystal as a result of displacement along the length of the crystal.

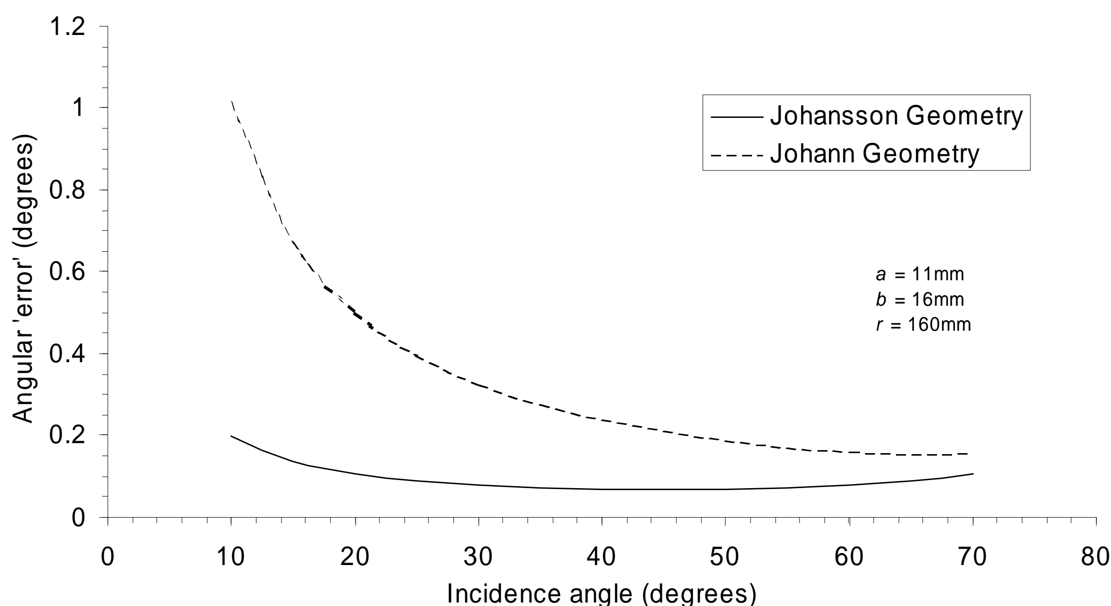

Fig. 8. Graph showing the relationship between the maximum angular error and incidence angle for both Johann and Johansson crystals.

Defocusing caused by displacement of the source

The sensitivity of the Bragg reflection to any angular deviation also has a very limiting effect on any displacement of the source (i.e. the point of impact of the electron beam on the sample): any deviation of this point in x, y or z will generally change the incidence angle of the X-rays at the crystal. Note that the x and y used here refer to axes relative to the (vertical) spectrometer, not those of the stage, with x being parallel the plane of its Rowland circle and y perpendicular to it (z is still the vertical axis).

Deviations from the Bragg angle as functions of x and z displacements of the source

$$\Delta\theta_z = \Delta z \cos\phi \Big/ 2r\sin\theta$$

and

$$\Delta\theta_x = \Delta x \sec\phi \Big/ 2r\sin\theta$$

where:
$\Delta\theta$ is the deviation from the Bragg angle,
Δz is the vertical displacement,
Δx is horizontal displacement in the plane of the Rowland circle,
ϕ is the takeoff angle of the spectrometer,
r is the radius of the Rowland circle,

θ is the angle of incidence.

The angular 'errors' are given by two very similar equations above. As can be seen both are functions of the incidence angle, but for a given value of θ the angular 'error' is directly proportional to the displacement. Fig. 9 shows that the sensitivity to displacement decreases with increasing incidence angle. Displacement in *y* has virtually no effect on the incidence angle and so, within the physical 'field of view' of the spectrometer, this has no effect.

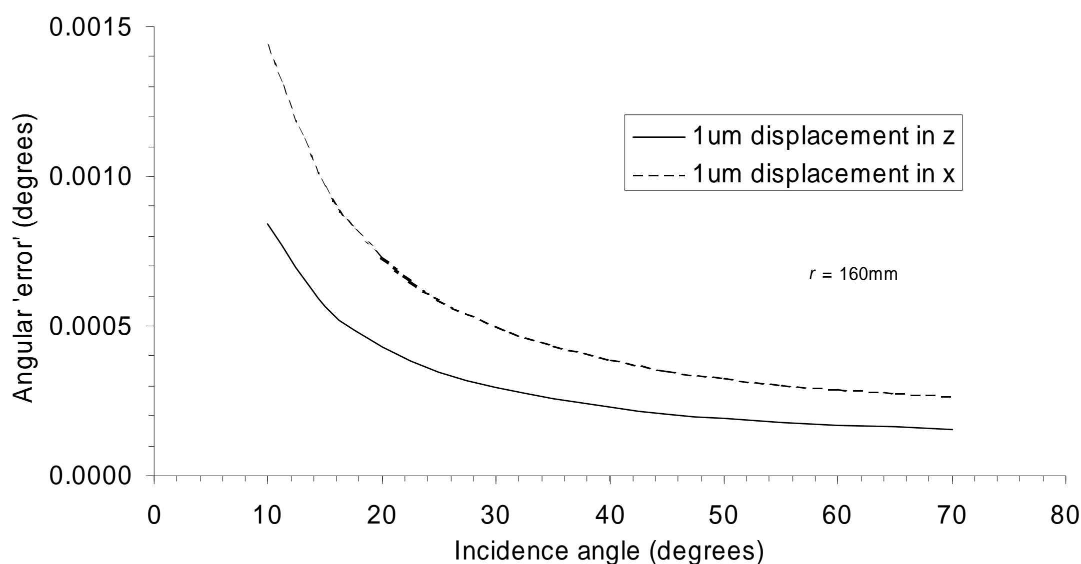

Fig. 9. Graph showing the relationship between the maximum angular error and incidence angle as a result of displacement of the source in *x* or *z*.

The sensitivity to *z* is usually not much of a problem, just requiring careful focussing, and at least partly explains why samples need to be polished flat for analysis. However, the defocusing along *x* can be very restrictive, for example limiting the size of area that can be mapped with a rastered beam. Whilst the above plots give the angular deviations it's more useful to determine the actual effect on count rates on your instrument.

Fortunately this is very easy to do. Fig. 10 shows line profiles for Si Kα acquired on a silica standard, using a TAP crystal on both vertical and inclined spectrometers, and a PET crystal on a vertical spectrometer. The profiles have been normalised to give the percentage decrease in count rate as a function of *x* or *z*-displacement from the focal point.

As can be seen the sensitivity to defocusing varies considerably for the three combinations of crystal and spectrometer orientation. In both *x* and *z*-displacements the PET crystal is less sensitive than the TAP crystal on vertical spectrometers since Si Kα is at a much higher angle on the PET (due to its smaller d-spacing). The inclined spectrometer, however, is

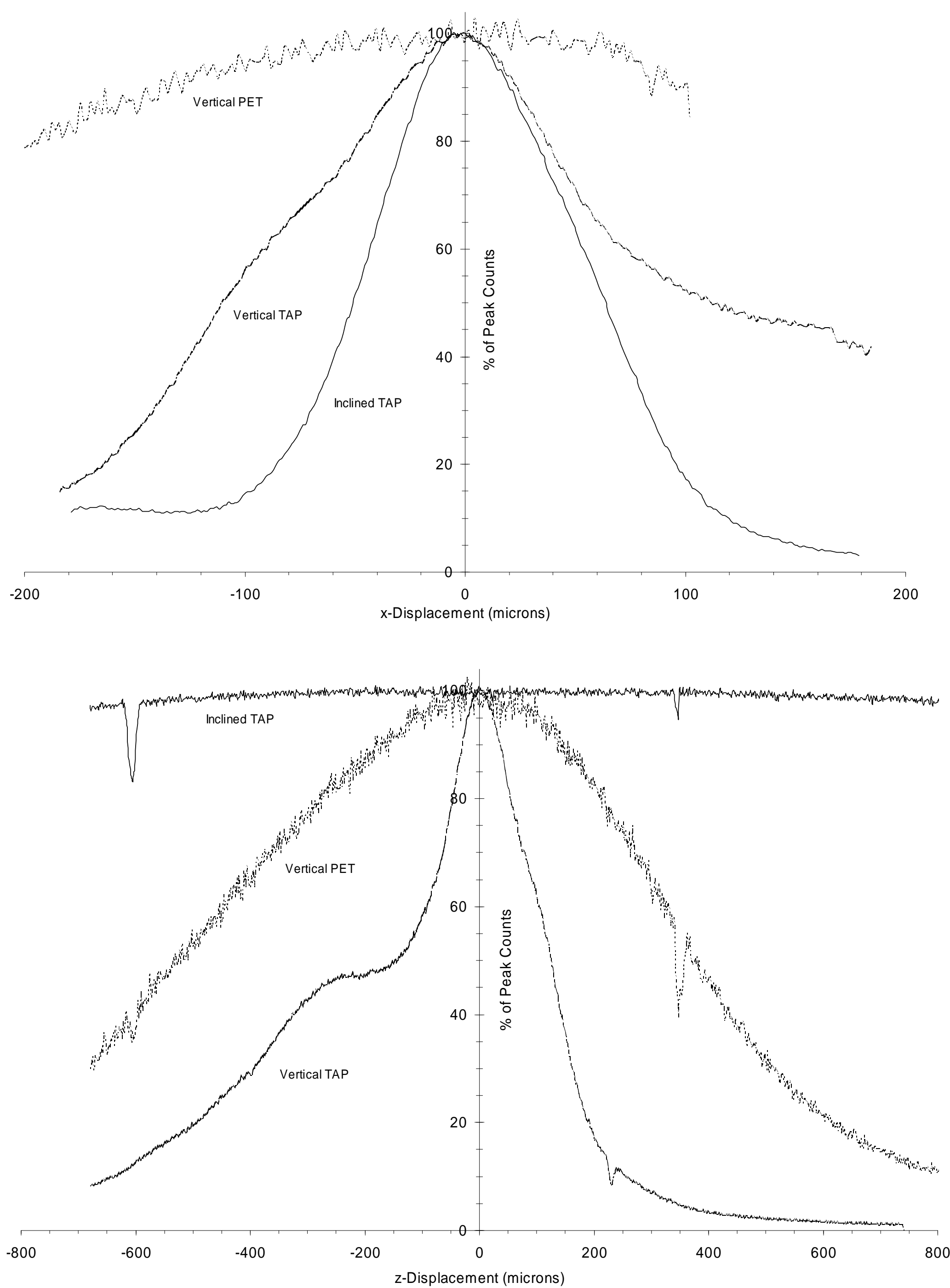

Fig. 10. Graphs showing effect on signal intensity as a result of displacement of the source in the *x* or *z* axes.

the least sensitive to *z*-displacement, but the most sensitive to *x*-displacement of the three combinations. This is because, on an inclined spectrometer the focussing axes are rotated so that the insensitive *y*-axis of the vertical orientation becomes the *z*-axis in the inclined spectrometer. Probably the only reason for having an inclined spectrometer is to use this

z-insensitivity to analyse 'rough' samples. The trade-off is the increased sensitivity in *x*, and the loss of an available spectrometer port (since the geometrical requirements of an inclined spectrometers usually mean that they occupy one port but obscure an adjacent one). Note, though, that the inclined geometry doesn't correct for any variation in X-ray intensity resulting from the sample surface not being perpendicular to the electron beam.

Spectral holes

These are features of the X-ray spectra produced by a WDS and result from the fact that the crystals used have lattice planes other than the ones wanted for filtering the incident X-rays. They resemble 'negative' peaks in an X-ray spectrum and are caused by reflection of the incident X-rays on the 'wrong' lattice planes, effectively diffracting the X-rays away from the detector. They can cause problems when selecting background positions. For example the background drops by about 10% on the LIF spectrum at a 2θ angle of 36.87°, where it is seen as a depression in the background level just below the Au Lα peak at 36.98°. Fortunately they're not a common feature (Fig. 11).

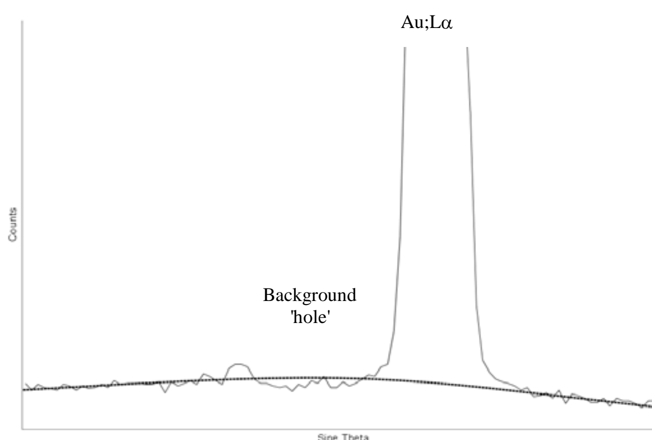

Fig. 11. Plot of portion of an X-ray spectrum acquired using an LiF crystal, showing the Au Lα peak and the background 'hole' next to it. The smooth curve shows the interpolated background.

The detector

Principle

The detector (Fig. 12) uses the principle of gas ionisation to measure the flux of X-rays being passed by the wavelength filter. It is comprised of a gas filled metal tube with an X-ray transparent window in one wall. A wire, insulated from the metal walls, runs along the central axis of the tube. X-rays entering the chamber ionise the gas, liberating electrons. A potential difference between the chamber wall (cathode) and the wire (anode) draw the ions to the chamber wall and the electrons to the wire, making a current flow. Each ion pair requires

25 - 30eV of energy to create, the number of ion pairs created (and therefore the current that is generated) is therefore proportional to the energy of the X-ray.

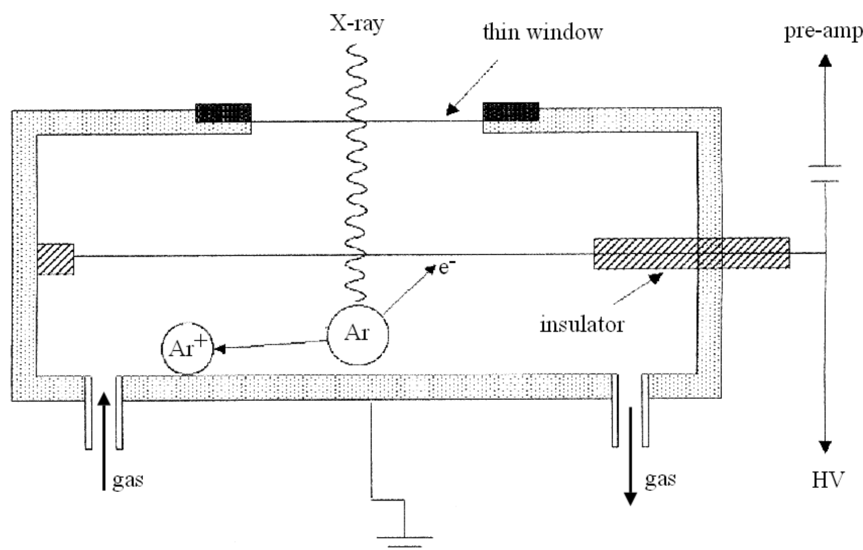

Fig. 12. Schematic diagram of a gas flow proportional counter. A sealed counter has all the same features except that the gas inlet and outlet are sealed during manufacture.

The potential difference between the anode and cathode has a secondary effect in that it accelerates the ion pairs, which in turn cause further ionisations en-route, effectively amplifying the signal. This effect is called the 'gas gain'.

There are three distinct 'gas gain' regions in a gas proportional counter (Fig. 13), controlled by the level of the applied potential: In the absence of any potential the ion pairs will simply recombine and no pulse will be measured. Applying a small potential will cause the ion pairs to migrate towards the anode and cathode, but recombination will still occur. The proportion of ions reaching the electrodes before recombining will increase with the applied potential until all do. At this point the gas gain value is one, i.e. all the pulse energy is measured, but there is no amplification. This is called the Ionisation Chamber region. The gas gain remains at one until the applied voltage is large enough to give the ions sufficient kinetic energy to ionise the counter gas en route to the electrodes. Once this happens the gas gain will start to increase proportionally with the applied potential. More importantly the energy pulse will still be proportional to the energy of the absorbed X-ray. This is called the Proportional Counter region and is the state that we try to maintain the detector in. Amplification values from 10^2 to 10^5 are possible in this region. Above about 10^5 though the number of ion pairs being generated becomes so large that they start to interact/repel and so the proportionality starts to break down until ionisation floods the whole length of the wire. This is the Geiger Counter region. Since the wire is saturated by any X-ray it has lost its energy resolution, and

also dramatically increases the dead-time of the counter (the time taken for the gas to recover enough to measure another incoming X-ray) making it unsuitable for EPMA use.

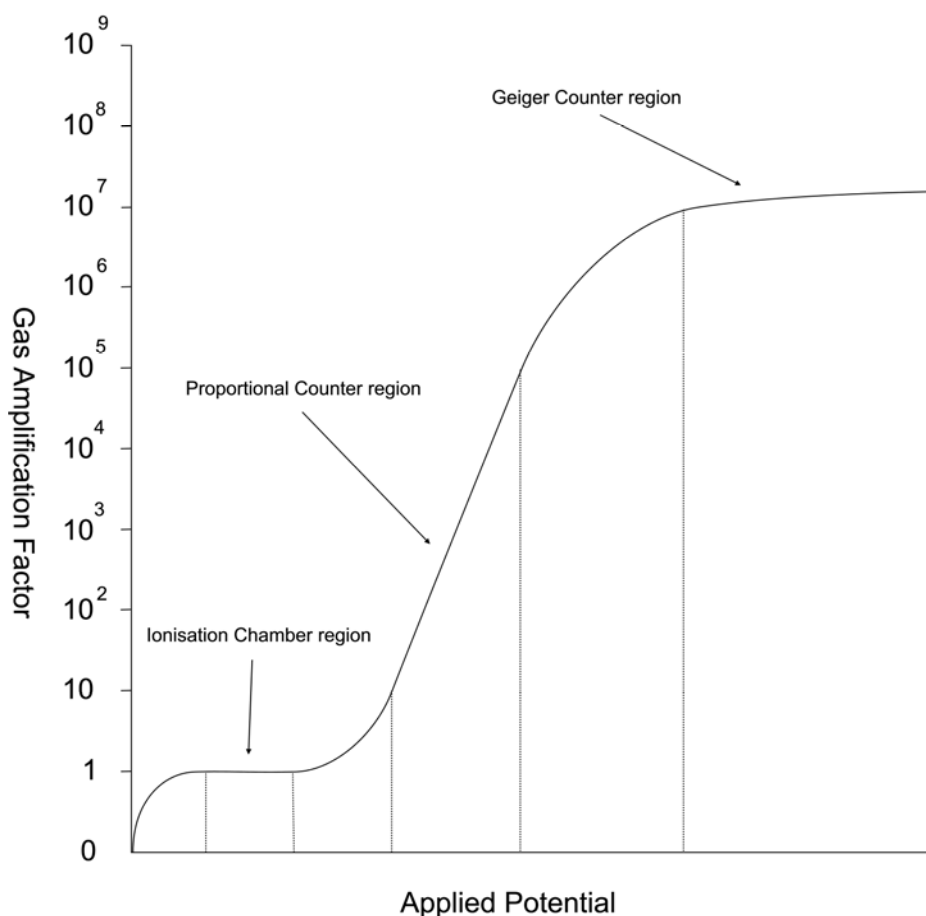

Fig. 13. Graph showing the three different regions of gas amplification behaviour as a function of the applied potential in a gas filled counter.

Counter gas

Potentially any gas can be used, but electronegative gases such as oxygen are less suitable because the negative ions formed have low mobility and so a high probability of recombination before reaching the anode (if this happens no pulse of current is generated and so the X-ray is not detected). This is not the case for the noble gases, which also benefit from higher gas gains at a given voltage. Argon is the most common choice, being relatively cheap. However, as a pure gas it's transparent to UV and so allows any photons emitted by gas excitation to reach the counter wall where they release extra electrons. This advances the onset of Geiger mode operation, reducing the level of useable gas gain. The addition of a polyatomic gas (usually 10 % of methane) increases the UV absorption sufficiently.

To be most efficient the gas should absorb all the incident X-rays (Fig. 14). At atmospheric pressure argon is effective at wavelengths above about 5 Å (i.e. lower energy X-rays). For the shorter wavelength X-rays (higher energies) Cameca still uses argon/methane but increase its high energy absorption by increasing the pressure to 2 - 3 atmospheres. However, the thicker window required for the increased pressure causes increased absorption of the lower energy (higher wavelength) X-rays. Jeol uses the denser gas xenon to increase absorption.

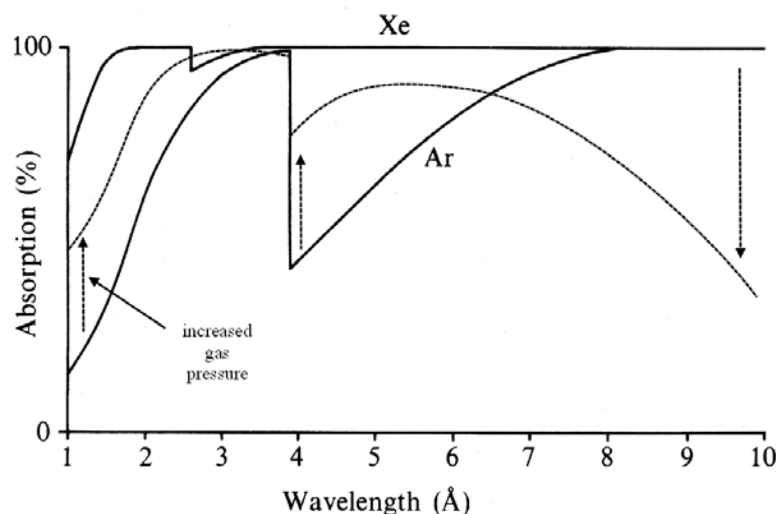

Fig. 14. Plots of the absorption curves for argon and xenon at atmospheric pressure, and the effect on argon's absorption as a result of increasing its pressure.

The purity of the gas is important, particularly with regard to oxygen and water vapour. Normal commercial supplies are generally sufficiently clean, but since any impurities tend to increase as the bottle becomes exhausted it's advisable to switch bottles before they are completely empty.

Entrance window

The purpose of the entrance window is to allow X-rays to enter the counter, whilst separating the counter gas from the vacuum of the spectrometer. To minimise the absorption of the X-rays by the window this needs to be as thin and as low density as possible. Fig. 15 shows the relative absorptions for some of the more common materials and thicknesses.

For the lower energy longer wavelength X-rays the absorption is more critical. For these X-rays the window may be supported by a metal grid. Whilst this reduces the effective area of the window by physical masking of the aperture, they allow for much thinner materials to be used. However, these are not gas impermeable. In order to overcome the gas leakage through

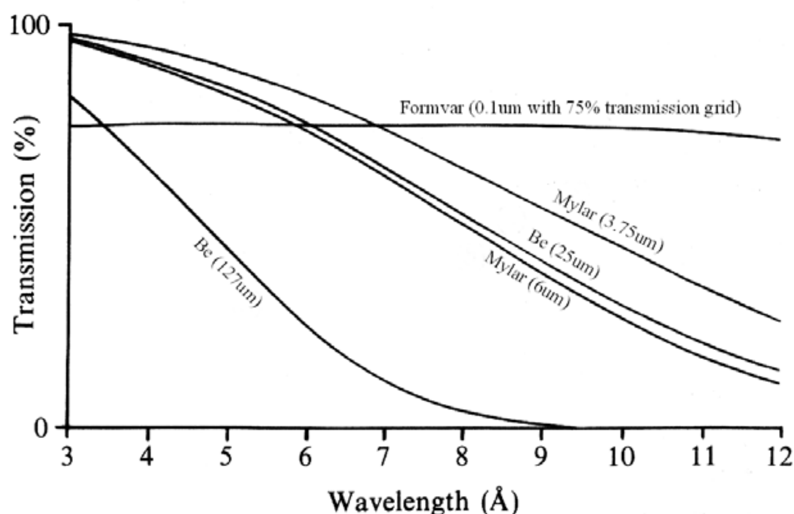

Fig. 15. Plots of the absorption curves for some common window materials and thicknesses.

the window the counter is fed with a slow bleed of gas. These are called gas flow counters. For their high pressure counters (for the higher energy shorter wavelengths) Cameca still uses this gas flow design, but Jeol's Xenon counters are 'sealed'. These are not replenished by a continuous flow, but rely on the impermeability of the window material to prevent the gas leaking away. I haven't heard any horror stories of such sealed counters having to be replaced, so the design obviously works.

Pulse height depression

As mentioned at the start of this section, the energy generated in the counter is proportional to the energy of the ionising X-ray. This 'pulse height' is usually measured as a voltage level. Plotting the voltage against intensity generates a roughly Gaussian curve. Note this is the energy spectrum for the X-rays being detected by the counter at a specific spectrometer angle, and should not be confused with the characteristic X-ray peaks that are the final output of the spectrometer. The area under this 'pulse height' curve gives the X-ray count rate detected by the spectrometer for the current angle. The signal to noise ratio of the counter is improved by setting a 'discriminator' level on the low voltage side of the peak, excluding the low energy pulses that result mainly from electronic noise and scattered X-rays. Further noise reduction can also be achieved by setting a second threshold on the higher energy side of the pulse height peak. The main benefit of this upper threshold is to exclude the higher energy pulses that result from higher order reflections from the crystal, i.e. for solutions to the Bragg equation for $n>1$. Fig. 16 shows the pulse height plot for a spectrometer position where second order Ag Lα overlaps with first order Al Kα in a sample where both Ag and Al are present in the analysis volume. The wavelength of Ag Lα, 4.1544 Å, is close to half that of Al Kα, 8.3393 Å, so two wavelengths of the Ag Lα X-rays will satisfy the Bragg condition at roughly the same position as one wavelength of the Al Kα X-ray. The diffracting crystal will therefore

not be able to discriminate between the two and will pass both X-rays to the counter. However, since the wavelength of the Ag X-ray is half that of the Al it will have twice the energy, producing the two distinct peaks in the pulse height measured by the counter. If no upper window is set between the two peaks both will be counted, leading to Ag being erroneously identified as Al. This windowing of the pulse height signal is called pulse height analysis.

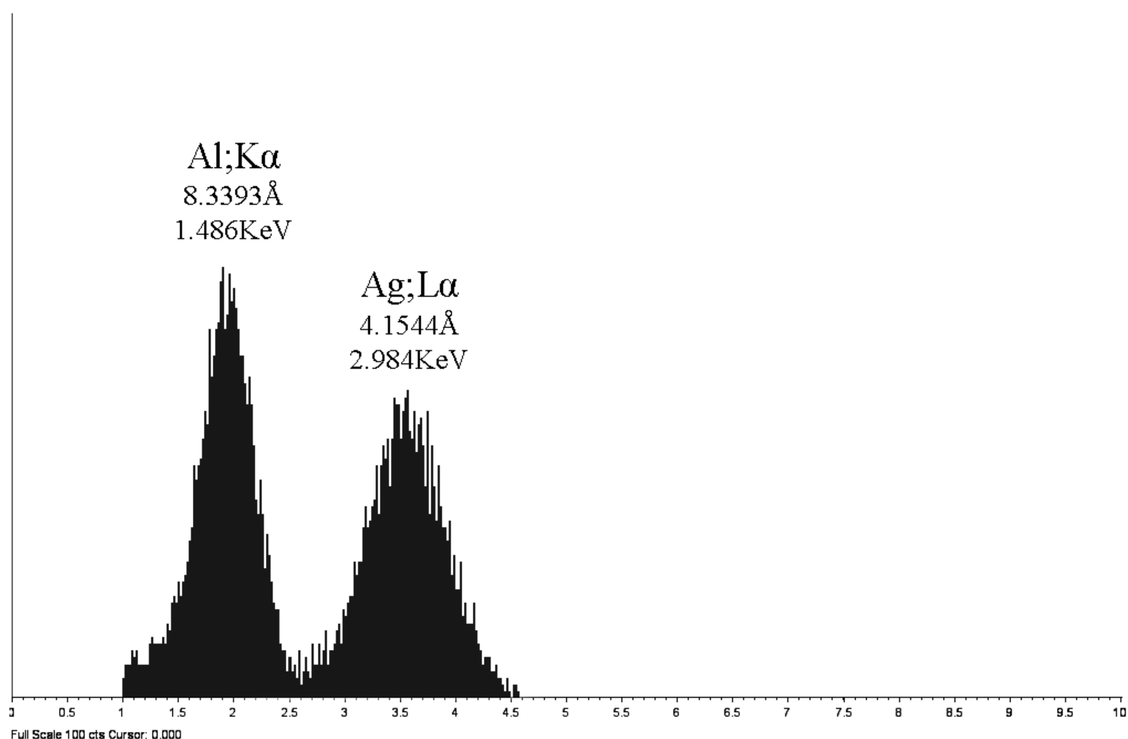

Fig. 16. Pulse height analysis plot showing both first and second order peaks.

At high X-ray fluxes the relationship between the X-ray energy and the pulse height becomes non-linear. The mechanism is not fully understood, but the effect is that, at high count rates, the pulse height curve is shifted to lower voltages. If a tight discriminator window is being used the pulse height curve can become cropped, causing a loss in the number of X-ray counts. The effect is reduced in modern instruments by using lower anode voltages and compensating for the lower resulting gas gain with low noise high gain preamplifiers.

A similar effect to pulse height depression is caused by temperature and pressure changes. This is because the gas gain varies with its density (which is a function of its temperature and pressure). A 1 mbar difference at atmospheric pressure will give roughly a 1 % change in the pulse height, whilst a 1 °C difference in temperature results in about a 3 % change. Fig. 17 below shows an example of pulse height peak shift as a consequence of pressure change.

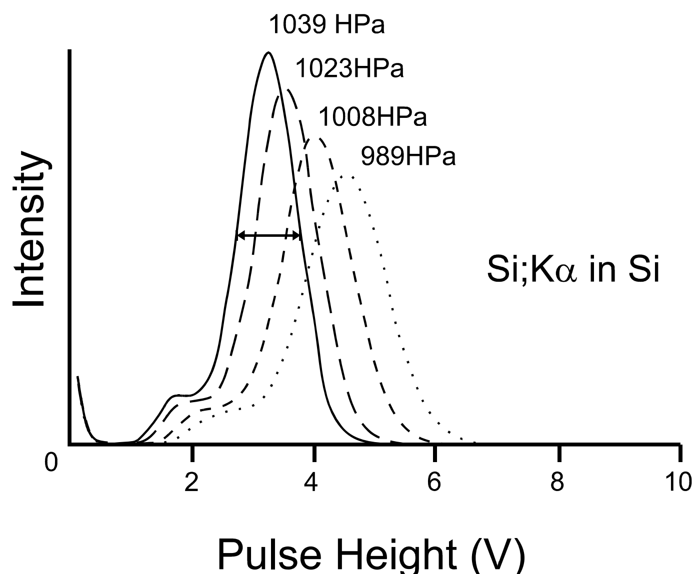

Fig. 17. Pot showing the effect of gas pressure on the pulse height analysis curve for Si Kα radiation from silicon.

Escape peaks

The K-shell absorption edge for Argon is 3.20 keV, and about 90 % of the incident X-rays with energies above this are absorbed by ionisation of this shell. The ' fluorescence yield' for this ionisation is 0.12, so 11 % (i.e. 90 % x 0.12) of the >3.20 keV ionisations result in the emission of an argon K-shell X-ray. Since an element is relatively transparent to its own characteristic radiation about half of these X-rays will escape re-absorption by the gas, and this energy will therefore be lost from those pulses. The result is a satellite peak, the 'escape peak', 2.96 keV below to the main pulse height peak (2.96 keV being the energy of the argon Kα X-ray) with a height about 5 % (i.e. 50 % of 11 %) of the main peak. If this escape peak lies below the discrimination window these counts will be lost, resulting in a 5 % decrease in the output X-ray intensity.

Xenon counters do not suffer from this effect since the K-absorption edge is outside the range of energies measured in EPMA. Whilst the L-absorption, at 4.78 - 5.45 keV, could produce 4 % of these ionisations as X-rays their re-absorption is relatively high so the resultant escape peak is negligible.

Practical performance

The overall efficiency of a WDS is a function of the solid angle of the crystal (i.e. the effective area of the crystal 'seen' by the source at any given angle), its reflectivity, and the detector efficiency.

The solid angle for a Johansson crystal is given by:

Solid angle of a diffraction crystal

$$\Omega = \sqrt{2}\left(2b/r\right)\sqrt{\left(R_i/\tan\theta\right)}$$

where:
Ω is the solid angle in steradians,
b is the half length of the crystal,
r is the radius of the Rowland circle,
R_i is the integrated reflection (the effective reflection angle in radians),
θ is the angle of incidence.

From Fig. 18 we can see that, not surprisingly, as the incident angle increases the source sees a more oblique view of the crystal and so its solid angle decreases.

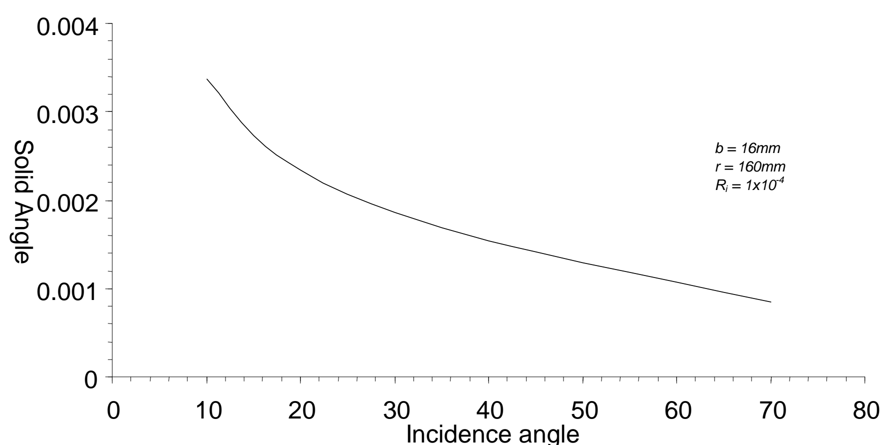

Fig. 18. Plot of the above equation, showing the relationship between solid angle and angle of incidence.

The crystal reflectivity varies both with angle and with material. Fig. 19 gives the curves for the three most common crystals, TAP, PET, and LIF. As with the solid angle we see that the values decrease with increasing incidence angle.

The efficiency of the detector is governed by its ability to absorb X-rays, and this is primarily a function of the counter gas and the energy/wavelength of the X-rays being absorbed. The graph showing the X-ray absorption curves for xenon and argon/methane at atmospheric pressure is plotted in Fig. 14 above in the section on counter gas. As can be seen argon/methane doesn't absorb efficiently at wavelengths below about 5 Å. The sharp rise just below 4 Å is the argon K absorption edge.

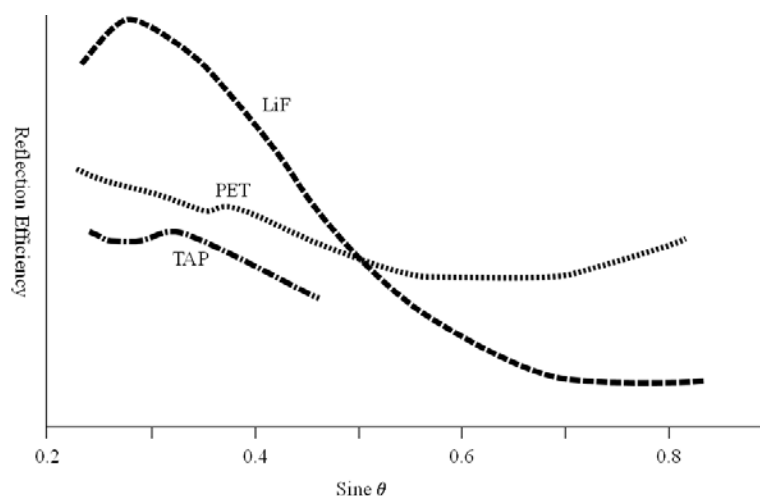

Fig. 19. Reflection efficiency curves for the three most common diffraction crystals.

The graph in Fig. 20 shows the relative performances of TAP, PET, and LIF crystals, derived from experimental data for Kα line intensities. In the regions where the curves overlap the crystal with the larger d-spacing gives the higher intensity. This is because, having a larger d-value, the Bragg equation shows us that the same wavelength will be diffracted at a lower incidence angle, where the spectrometer is more efficient. The trade-off, as we saw from the discussions on resolution above, is that for Johann geometry the resolution will be worse than for the smaller d-spacing crystal diffracting at the higher incidence angle. Note that a step is present in the low pressure PET data at about 3 keV. This is caused by the Ar absorption edge in the gas flow counter. The step is present but less pronounced in the high P PET data because, as we saw in Fig. 14 above, increasing the pressure of the gas suppresses the effect of the absorption edge.

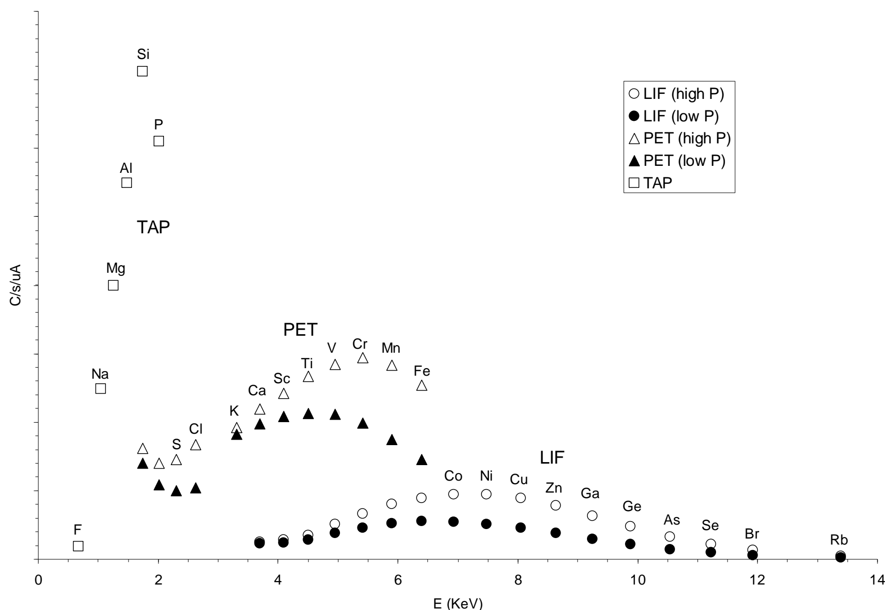

Fig. 20. Plots from experimental data showing the relative count rates as a function of atomic number for Kα X-ray emissions for TAP, PET and LiF crystals at a given beam current. Data for both low and high pressure gas flow proportional counters are given for the LiF and PET crystals.

Summary

The performance of the WD spectrometer can be summarised in the following diagram:

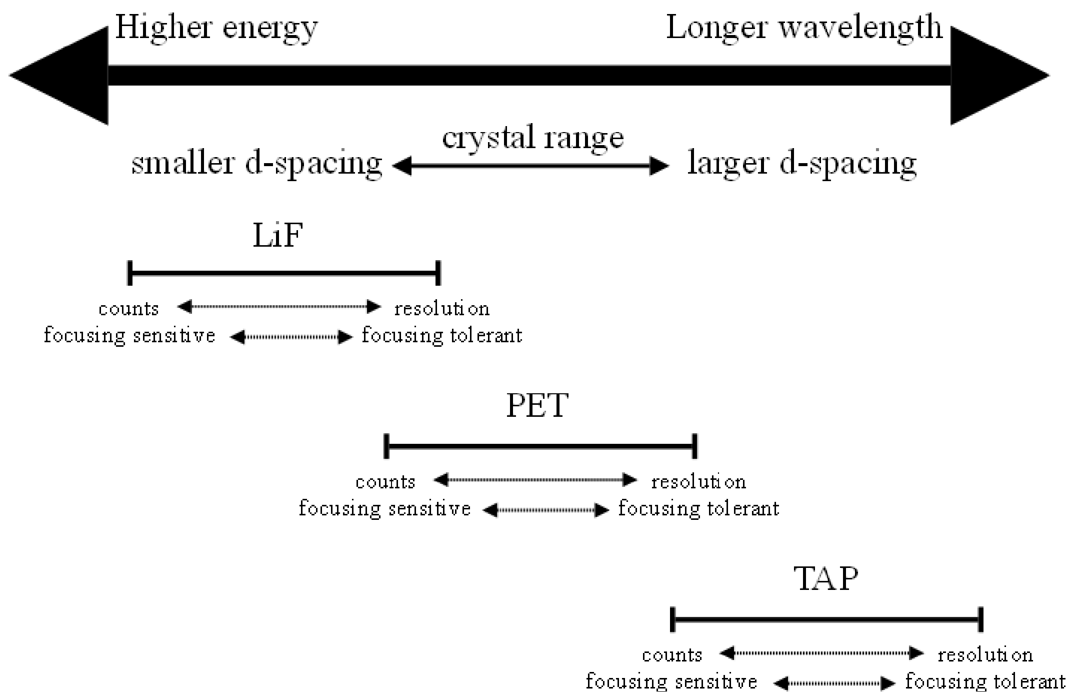

PART 2 - ENERGY-DISPERSIVE SPECTROMETERS

Principals of operation

In solid state energy dispersive spectrometers filtering and detection are combined in a single device (Fig. 21). This uses the ionisation of the solid detector material to both count the number of incident X-rays and measure their energy. This is the same process that the gas proportional counter uses in the WDS, and in fact these can be used as EDS detectors but are rarely seen since the solid state detectors offer far better energy resolution. The main material used is silicon, but germanium is also common now. The theoretical energy required for each ion pair is 1.1 eV for silicon (0.60 eV for germanium), but losses due to exciting lattice vibrations mean the real energy is nearer 3.8 eV (2.9 eV for germanium). Comparing this with the 25 eV of the gas flow detector we see that considerably more charge carriers will be generated in the solid state detector, lowering the statistical fluctuations and therefore giving better energy resolution. For example, a silicon Kα X-ray, with an energy of 1.74 keV will generate 64 ion pairs in a gas proportional counter, but 470 in silicon, and 600 in germanium.

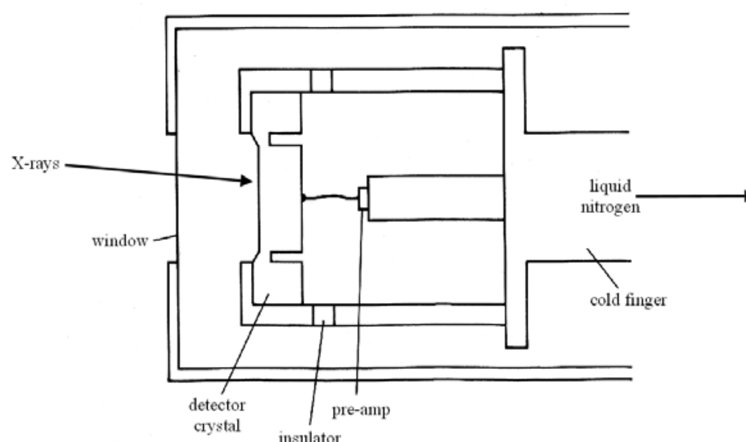

Fig. 21. Schematic showing the principal components of a solid state EDS detector.

Perfectly pure Silicon theoretically has all the physical qualities to act as an EDS detector. However, the purest silicon available contains enough impurities, particularly Boron, to lower the high intrinsic resistivity of the silicon to the point where ion pairs are created too easily by thermal excitation. These ‘leakage currents’ raise the detector noise to unacceptable levels. The addition of just the right amount of lithium neutralises the effect of the boron, restoring the resistivity (see Reed for a description of the mechanism). The lithium is ‘drifted’ through the silicon crystal using an applied electric field. The field creates a constant lithium concentration within the silicon which exactly balances the effects of the impurities. This gives the detector its name of lithium drifted silicon or Si(Li) detector (pronounced ‘silly’). The uncompensated edges of the silicon are trimmed off.

Solid state detectors have no gas gain to amplify the pulse signal, so a low noise preamplifier has to be fitted directly to the back of the crystal, and the crystal is cooled (usually with liquid nitrogen) to reduce thermally induced noise as much as possible. The cooling also prevents diffusion of the lithium. Electrical contact with the front of the crystal is via an evaporated layer of gold. Since the chilled detector would act as a 'cold finger', condensing out any hydrocarbons in the chamber, the end face is usually also thermally isolated from the chamber by a thin window.

Removing the need for a separate filter greatly simplifies the mechanics of the detector, and gives it two advantages over the WDS; firstly there are no defocusing problems. In the WDS all the focussing limitations result from the geometrical requirements of the diffraction crystal. The EDS works by line of sight, collecting all the X-rays that fall on the detector face. Secondly, the entire energy spectrum is covered by the same detector, and is acquired simultaneously. Obviously there are penalties to pay for these benefits otherwise we would all have thrown our WD spectrometers away. By far the biggest limitation of the EDS is its resolution.

Factors affecting resolution

Noise

EDS resolution is primarily controlled by statistical variations in the count rates and by the noise level in the detector and preamplifier. The level of statistical variation is dependant upon the number of ion pairs generated by each X-ray - the more ion pairs created the smaller the uncertainty in the energy level due to random fluctuations. The preamplifier noise is affected by the capacitance of the detector, which increases with size. A smaller detector will therefore give better resolution, but at the expense of a smaller solid angle and therefore a smaller X-ray collection area. The result is a resolution of the order of 100 eV, which is an order of magnitude poorer than that for WDS (Fig. 22).

Incomplete charge collection

Any ion pairs generated but not collected result in energy lost to the pulse and produce a broadening of the low energy side of the X-ray peak (Fig. 23). This doesn't usually cause any problems with identifying peaks, but does cause difficulties with quantification, both with correctly modelling the shape of the peak and with modelling the background. There are several mechanisms which result in this loss:

- Silicon dead layer

  Charge collection in the first 0.2 μm or so of the detector crystal is very low. In this region the lithium is oxidised and so doesn't fully charge compensate the boron. The result is that X-rays absorbed in this region, primarily low energy X-rays, are not detected. This produces a jump in the detector efficiency and a resulting strong step in the background at 1.84 keV. The mechanisms acting in this layer are not fully understood, but it is thought that charge carriers migrate the short distance to the front face rather than travel the full thickness of the crystal under the influence of the bias voltage.

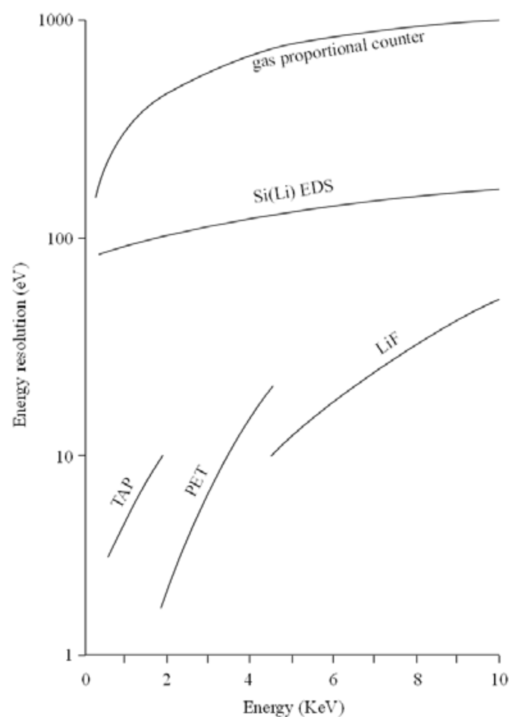

Fig. 22. Graph showing relative resolutions of gas proportional counters, Si(Li) EDS, and TAP, PET and LiF crystals. The lower the resolution value, the better the resolution.

Fig. 23. Plot of an experimentally acquired X-ray peak (open circles) and a fitted Gaussian curve (closed circles), showing the low energy tail in the experimental curve which results from incomplete charge collection.

- Trapping

  Impurities and defects in the detector crystal can temporarily trap charge carriers, releasing them after the main energy pulse has been measured. Modern crystals are relatively pure and have few defects so this mechanism now tends to be less significant.

Escape peaks

These result from a very similar mechanism to that in gas proportional counters: X-rays with energies higher than the silicon K-absorption edge at 1.841 keV might produce a silicon Kα X-ray. These have a large enough path length, having a 10 % chance of travelling 30 μm before being absorbed, that some will escape the detector entirely. If this happens the resulting energy pulse is reduced by the 1.739 keV, the energy of the silicon Kα X-ray, producing a peak in the energy spectrum 1.739 keV below the parent peak.

The intensity of the escape peak decreases with increasing energy since the deeper the X-ray is absorbed the less likely any generated silicon Kα is to escape. However they are generally less than 1 % of the parent peak and so may only be apparent for major elements. The actual values will depend on your individual detector, and will change with age. The main danger is that, unlike the WDS where pulse height analysis filters these escape peaks out, in the EDS they appear in the final spectrum where they may be mistaken for, or interfere with, a true element peak. Table 1 shows the intensities of some common escape peaks and their overlaps. A similar escape peak is generated by germanium crystal detectors.

Table 1. Intensities of some common escape peaks and their overlaps.

Element	Kα line (KeV)	Escape Peak (KeV)	Intensity (% of Kα)	Overlapping with: (KeV)
P	2.013	0.274	1.40	B (0.185), C (0.282)
S	2.307	0.568	1.30	O (0.523)
K	3.313	1.573	0.91	Al (1.487)
Ca	3.690	1.951	0.78	P (2.013)
Sc	4.089	2.349	0.67	S (2.307)
Cr	5.412	3.672	0.40	Ca (3.690)
Mn	5.895	4.155	0.33	Sc (4.089)
Cu	8.041	6.301	0.16	Fe (6.400)
Zn	8.631	6.891	0.13	Co (6.925)

Internal fluorescence

This is effectively the opposite process to escape peaks, being the excitation of silicon Kα radiation within the detector. There are two processes that can cause this. The first is production of an Auger electron and a silicon Kα X-ray in the detector dead layer. If the Auger electron is 'lost' in the dead layer but the silicon K X-ray is absorbed in the active part of the detector the measured energy of the pulse is only that of the silicon Kα X-ray, i.e. 1.739 keV. In other words, regardless of what element's X-ray has been absorbed, the resultant peak is for silicon Kα. The second mechanism is the direct excitation of the silicon Kα radiation, either by background radiation (which is relatively high in the region of the silicon absorption edge) or by high energy backscatter electrons reaching the counter. This

latter mechanism should only be possible in ultra thin or windowless detectors since normal detector windows should absorb stray electrons. Whichever mechanism is the main cause, these spurious silicon Kα peaks will only contribute about 0.2 % to the silicon peak in silicate analyses. However, it may cause a real problem when identifying or quantifying trace silicon levels.

Dead time

Dead time is the period immediately following the absorption of an X-ray during which the system measures the energy of the pulse and clears itself ready for the next. The length of this period is controlled by the time constant (effectively the integration time) of the amplifier. As this is reduced the dead time shortens and so higher count rates can be processed (Fig. 24). However, the noise level in the pulse increases and so its resolution decreases. There is therefore a trade-off between count rate and resolution. Modern digital pulse processors allow the user to select different time constant values depending on whether counts or resolution are more critical for a given analysis.

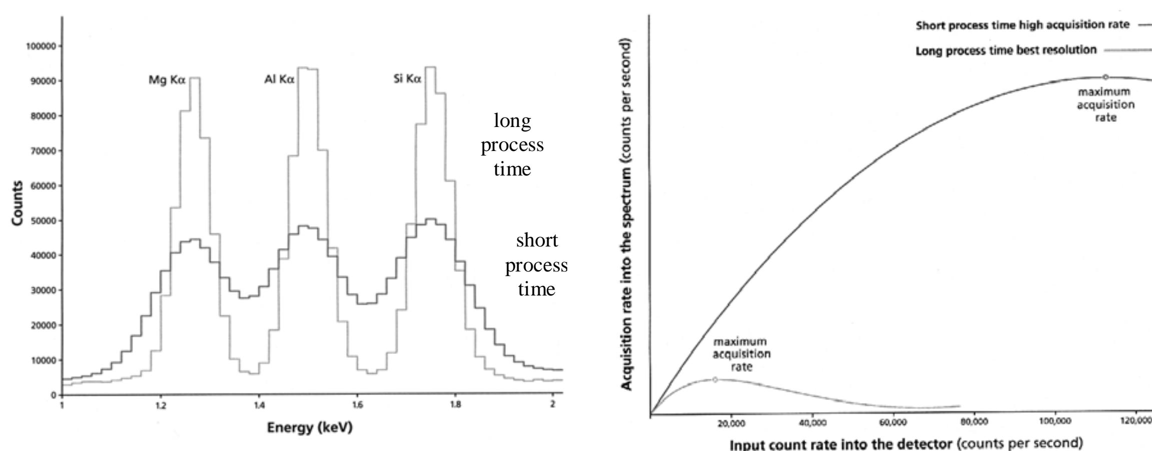

Fig. 24. Plots showing the effect on resolution and achievable count rates for the same EDS detector but using long and short process times.

Pulse pile-up

If two X-rays are absorbed in the detector effectively at the same time (i.e. the second pulse during the rise time of the first) then the detector will only see one event with an energy equal to the sum of the energies of the two X-rays. This produces two problems; firstly the parent elements will have lost these counts and so their peaks will be smaller than they should be, and secondly a ‘sum peak’ will appear in the spectrum (Fig. 25). Modern high speed electronics can now discriminate such events, but you may need to look out for these artefact peaks if you use an older system.

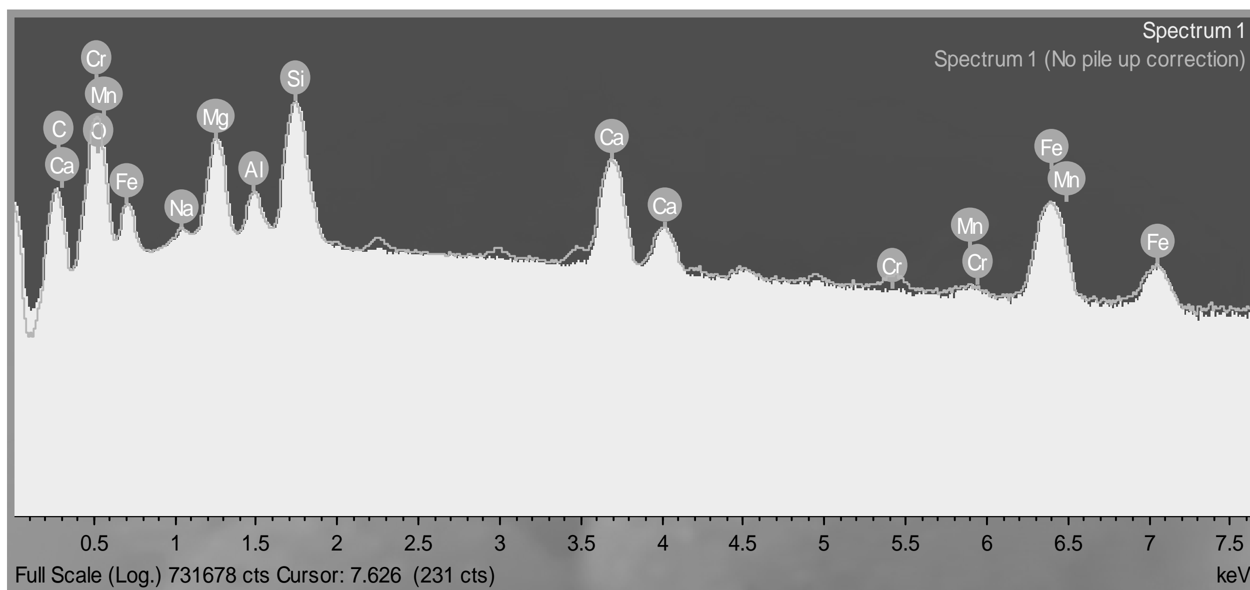

Fig. 25. EDS spectra showing the presence of pile-up peaks in the uncorrected spectrum (line) relative to the pile-up corrected spectrum (solid). Note that the vertical axis is a log scale.

Efficiency

The overall efficiency of the ED detector is a function of its solid angle, absorption from the counter window and gold contact layer, and the absorbing efficiency of the detector crystal.

Since there is no benefit from having the detector face at any angle other than perpendicular to the X-ray paths the solid angle is given simply by the active surface area of the crystal divided by the square of its distance from the X-ray source. This is typically about 0.004 steradians.

Absorption by the counter window and gold contact layer is a function of the X-ray energy, but increases strongly for energies below about 1 keV. This is why detectors which can detect elements below sodium Kα radiation at 1.04 keV need to have either ultra-thin windows or be windowless. Above about 2 keV absorption drops to only a few percent or less.

The detector crystal is very effective at absorbing the incident X-rays, losing only a few percent to incomplete charge collection etc… up to energies of about 20 keV. Above this losses start to increase due to X-rays passing straight through the crystal, typically about 3 mm, without being absorbed.

The overall detector efficiency as a function of atomic number (which is equivalent to energy in this data) is shown in Fig. 26.

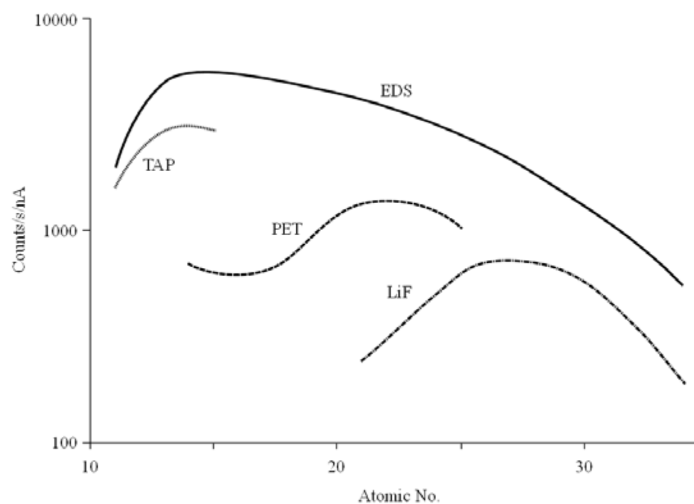

Fig. 26. Plots from experimental data showing the relative count rates as a function of atomic number for Kα X-ray emissions fo rSi(Li) EDS, and TAP, PET and LiF crystals at a given beam current.

Silicon drift detectors

The newest readily commercially available ED technology is the SDD or Silicon Drift Detector. This is based on a wafer of n-type Si, as is used in the semiconductor industry. Semiconductors are usually doped to provide a surplus of electrons and holes. However for X-ray measurement it isn't beneficial to measure the small increase in electron-hole pairs generated by the ionisation from an absorbed X-ray against a high background of pre-existing electron-hole pairs. In the SDD a bias voltage is applied to effectively sweep the electron-hole pairs out to produce a fully depleted material through the full thickness of the wafer. Fig. 27 shows a cut-away schematic through a typical SDD. This design creates a very charge 'clean' material with a very low leakage current, even at room temperatures. Resolutions of better than 300 eV (at Mn Kα) can be achieved at room temperature but with only moderate cooling, such as the ~35° cooling that can be achieved with a single stage Peltier, SDD can now match Si(Li) (~127 eV). This removes need for liquid Nitrogen and allows for very fast start-up from 'hot'.

By 'shaping' the bias applied between the field rings all the electrons generated anywhere in the wafer 'drift' towards the small collecting anode. Fig. 28 shows the calculated field in the wafer in Fig. 27. The horizontal portion at the back of this curve is the 'back' face of the wafer, which is the entrance face for the incoming X-rays, and the read-out anode is at the minimum. From this we can see that, no matter where an electron cloud is formed, it will 'drift' to the anode. Drift is a very misleading term, implying a very leisurely process. In fact for the size of wafer typically used, only 300 μm thick by only 2 - 3mm diameter, it takes less than 100 ns for all electrons to reach the anode.

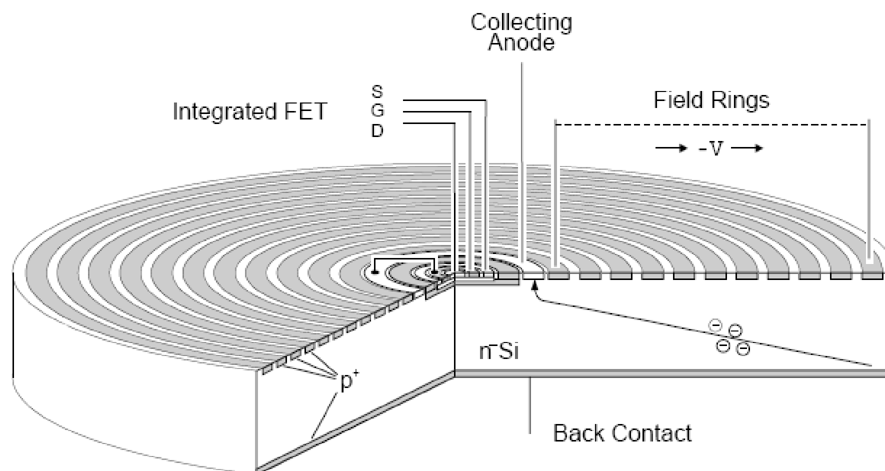

Fig. 27. Cut-away schematic showing the components of a silicon drift detector.

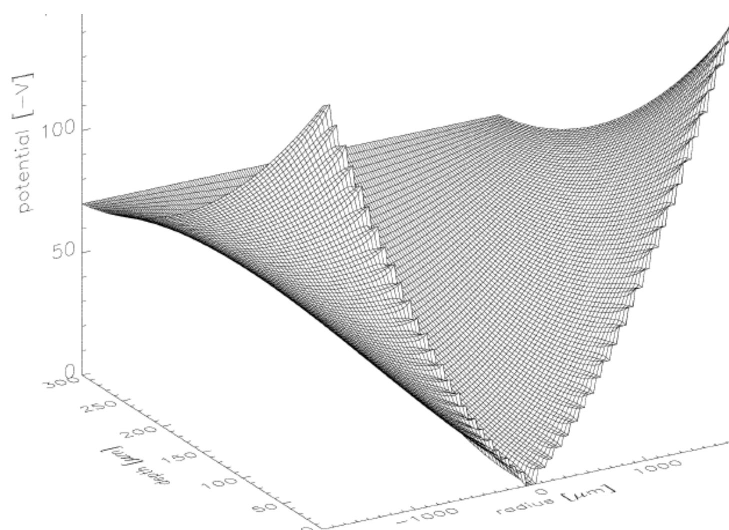

Fig. 28. Calculated field in the wafer shown in Fig. 27 above. The horizontal field surface at the back of the plot is the 'back contact' face of the wafer and the curve minimum is the collecting anode.

This configuration results in an extremely small capacitance, which is effectively independent of the size of the wafer, unlike in Si(Li) where capacitance increases with size. A reduced capacitance generates a shorter rise time and higher amplitude on the read-out energy pulse per collected electron. This results in an increased signal to noise ratio and therefore an improved resolution at higher count rates. Silicon drift detectors can achieve 100 Kcps without any appreciable drop in resolution. Fig. 29 shows experimental data for a silicon drift detector of the type of configuration shown in Fig. 27 above. Shaping times range from 0.5 - 1 µs, reducing to 100 ns at high count rates (>100 Kcps) to avoid pulse pile-up. This is about

100 times less than those used in Si(Li). These high count rates achievable make SDD particularly useful for mapping and for combined ED-WD working.

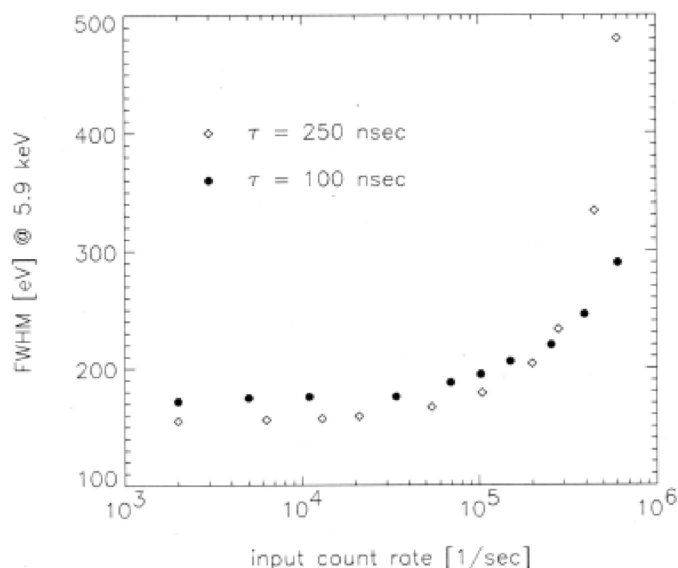

Fig. 29. Experimental data showing resolution as a function of count rate for a silicon drift detector.

The semi-conductor nature of this detector means that the pre-amp stage, the FET, can be integrated directly onto the back face. This greatly simplifies the detector package but more importantly for performance minimises the capacitance overhead of the pre-amp, as well as reducing electrical pick-up and microphonic (vibration) effects. Also, unlike in Si(Li) where the charge built up from successive X-ray events needs to be periodically re-set, the SDD self re-sets at a given voltage level. This simplifies the electronics, removes the need for any clock-overhead, is self compensating for changing count rates, and means that only simple DC voltage supplies are needed.

Overall the SDD wafer is almost a detector on a chip, requiring only DC voltage supplies, and little cooling, making it versatile, compact, robust and (relatively) cheap whilst providing very high count rate capabilities.

However, these benefits need to be balanced by the less favourable features of SDD:

- High energy performance: The wafer is typically 300 μm thick, compared to 3 - 5mm for Si(Li), meaning that higher energy X-rays can pass through without being absorbed. This results in poorer high energy performance. At 10 keV SDD can achieve better that 90 % efficiency, but by 20 keV this drops to the region of 50 %.
- Pulse pile-up: As in Si(Li) detectors pulse pile-up occurs in the SDD, especially given the high count rates achievable by SDD. However this is partly compensated for by the very short shaping times.

- FET 'burn': Having the FET in the centre of the back of the wafer means that it is prone to damage from high energy X-rays not absorbed by the wafer, especially in applications that require continuous high count rates. At least one manufacturer now produces a tear-drop shaped configuration, with the collecting anode moved to outside the path of the X-rays.
- Incomplete Charge Collection (ICC): SDD can collect electrons generated anywhere in the n-type body of the wafer. However, the p+ front contact layer acts like the 'dead layer' in a Si(Li) detector, reducing the efficiency and energy resolution for low energy X-rays. At present the low energy performance doesn't yet match that of Si(Li), but this may improve. It's only been in the last year or so that SDD has achieved the same resolutions as Si(Li) at Mn;Kα.
- Ballistic defect: As the electron cloud 'drifts' towards the collecting anode it starts to spread out. The very short shaping times possible (and sometimes essential) in the SDD mean that when they begin to approach the drift time of the electron cloud chopping can occur, causing an effect similar to ICC (i.e. low energy tailing and shelving). This is one of the drawbacks of the longer path length of the tear-drop configuration used to avoid FET burn.

SUMMARY

ED spectrometers are far simpler and quicker to use than WD spectrometers, not having any need to select diffraction crystals or choose between high or low pressure detectors. The penalty to pay is much poorer resolution (so peak overlaps are a serious problem), poorer peak to background ratio (so detection limits poorer) and a greater number of artefacts in the spectrum (e.g. escape peaks and sum peaks). Also, whilst the count rate for a given beam current is higher than for WDS, the detector will saturate at much lower total count rates than WDS, and these counts are spread over the entire spectrum. However, this is partly balanced by the fact that the total counts under a peak are used rather than just the peak maximum as in WDS. The advent of silicon drift detectors, which allow much higher count rates to be processed, means that this need not be as much of a problem now.

The general rule of thumb is that where a high degree of quantitative accuracy is required, or where the chemistry is complex (i.e. prone to overlapping peaks), or low detection limits are important, the WDS should be the tool of choice. Where speed is more important, or high analytical precision is not necessary then the EDS is a very valuable tool.

ACKNOWLEDGEMENT

I would especially like to thank Stephen Reed for being at hand on the end of an e-mail to answer questions, and for giving his time to proof read this document for me.

REFERENCES

I made extensive use of papers presented by numerous authors at EMAS meetings, but took many of my facts and diagrams from the following papers:

[1] C.G. Darwin (1914) *Phil. Mag.*, **27**, 675.

[2] S.J.B. Reed (1993) *Electron Microprobe Analysis* (2nd edition). Cambridge University Press.

[3] S.J.B. Reed (1997) *European Microbeam Analysis Society 5th European Workshop.* (Torquay, 11 - 15 May 1997) Book of Abstracts.

and from on-line documents at:

http://darkwing.uoregon.edu/~epmalab/pdfs/

and

www.oxinst.com/pdf/

© British Crown Copyright 2008/MOD